Applied Surface Science 268 (2013) 327–331

Contents lists available at SciVerse ScienceDirect

Applied Surface Science

journal homepage: www.elsevier.com/locate/apsusc

Structure and electrical properties of Mn doped $Bi(Mg_{1/2}Ti_{1/2})O_3$-$PbTiO_3$ ferroelectric thin films

Longdong Liu[a], Ruzhong Zuo[a,*], Qian Sun[a], Qi Liang[b]

[a] Institute of Electro Ceramics & Devices, School of Materials Science and Engineering, Hefei University of Technology, Hefei, 230009, PR China
[b] School of Electronic Science & Applied Physics, Hefei University of Technology, Hefei, 230009, PR China

ARTICLE INFO

Article history:
Received 28 June 2012
Received in revised form
12 December 2012
Accepted 17 December 2012
Available online 22 December 2012

Keywords:
Thin films
Sol–gel
Mn doping
Electrical properties

ABSTRACT

The Mn doped $0.63Bi(Mg_{1/2}Ti_{1/2})O_3$–$0.37PbTiO_3$ (BMT–0.37PT–*x*Mn, *x* = 0–0.01) thin films were deposited on Pt(1 1 1)/Ti/SiO_2/Si substrates by a sol–gel method. The effect of the Mn doping concentration on the structure and electrical properties of BMT–0.37PT thin films was studied. The X-ray diffraction data indicate that the B-site Mn substitution does not change the perovskite structure of the films. The X-ray photoelectron spectra show that Mn ions mainly exist as Mn^{3+} except for a few as Mn^{2+} for the 1 mol% Mn doped BMT–0.37PT film. Moreover, it was found that the addition of a small amount of Mn effectively reduces the dielectric loss and improves the resistivity of the films. The BMT–0.37PT–0.005Mn film exhibits lower leakage current density than the undoped BMT–0.37PT film such that saturated hysteresis loops can be achieved. As a result, the BMT–0.37PT–0.005Mn film exhibits the largest permittivity ($\varepsilon_r \sim 1271$ at 1 kHz) and remanent polarization ($P_r \sim 17.4\ \mu C/cm^2$ at 100 Hz) in all studied compositions.

1. Introduction

Much attention has been recently given to the ferroelectric thin films with high Curie-temperatures (T_c) because both high electrical performances and good temperature stability are required for applications in automotive, aerospace, and related industries [1–3]. Some $BiMeO_3$–$PbTiO_3$ and $Bi(Me1,Me2)O_3$–$PbTiO_3$ solid solutions have been widely studied including $BiScO_3$–$PbTiO_3$ (BS–PT) [4], $Bi(Ni_{1/2}Ti_{1/2})O_3$–$PbTiO_3$ (BNT–PT) [5], and $Bi(Mg_{1/2}Ti_{1/2})O_3$–$PbTiO_3$ (BMT–PT) [6]. BS–PT ceramics close to a morphotropic phase boundary (MPB) exhibit a high T_c (450 °C) and excellent piezoelectric properties (piezoelectric constant $d_{33} \sim 460$ pC/N and planar electromechanical coupling factor $k_p \sim 56\%$) [4]. 0.51BNT–0.49PT compositions possess a T_c of >400 °C and good piezoelectric properties [5]. $(1-x)$BMT–*x*PT ceramics were also been reported to have a relatively high T_c (~430 °C), good piezoelectric properties ($d_{33} \sim 225$ pC/N), and high remanent polarization ($P_r \sim 38\ \mu C/cm^2$) for the MPB composition ($x \sim 0.37$) [6]. However, the potential applications of BS–PT and BNT–PT systems were limited by the high cost of scandium sources, and the relatively high conductivity and dielectric loss, respectively. By comparison, BMT–PT exhibits better potentials for high-temperature device applications because of its high T_c, good electrical properties and low cost.

In our previous work, the MPB BMT–PT thin films were reported to exhibit excellent dielectric and ferroelectric properties with dielectric constant $\varepsilon_r = 1477$ and remanent polarization $P_r = 17.8\ \mu C/cm^2$ at 1 kHz [7]. However, the hysteresis loop of BMT–0.37PT films cannot be saturated owing to the relatively high electrical conductivity. This phenomenon has also been found in bulk ceramics [6,8]. The leakage current of ferroelectric thin films could seriously hinder their applications because it would degrade the long-term reliability of the storage elements and the refreshing time, induce large power consumptions and further give rise to the fatigue failure [9–11]. Therefore, it is essential to improve the electrical resistivity of BMT–PT thin films.

It is known that doping is an effective and simple method to tailor electrical properties of ferroelectric thin films. It has been demonstrated that the Mn doped ABO_3 perovskite ferroelectric thin films showed a reduction of the dielectric loss and an enhancement of the resistivity value [12–14]. In this work, the Mn-doped 0.63BMT–0.37PT (BMT–0.37PT–*x*Mn, *x* = 0.0, 0.002, 0.003, 0.005, and 0.01) thin films were fabricated on Pt(1 1 1)/Ti/SiO_2/Si substrates by a sol–gel method. The effects of the Mn doping contents on the structure, dielectric, ferroelectric properties and leakage current characteristics of the high-temperature thin films were investigated.

2. Experimental

According to the stoichiometry of BMT–0.37PT–*x*Mn films, 10 mol% excess Pb and Bi were used to compensate for

* Corresponding author. Tel.: +86 0551 2905285; fax: +086 0551 2905285.
E-mail address: piezolab@hfut.edu.cn (R. Zuo).

0169-4332/$ – see front matter © 2012 Elsevier B.V. All rights reserved.
http://dx.doi.org/10.1016/j.apsusc.2012.12.087

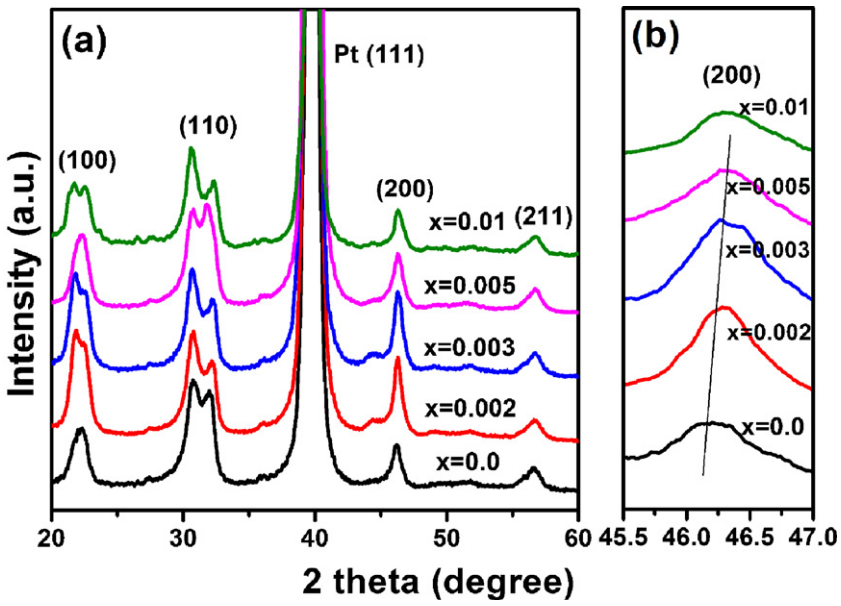

Fig. 1. (a) XRD patterns of the BMT–0.37PT–*x*Mn thin films annealed at 675 °C for 30 min, and (b) locally magnified (2 0 0) diffraction peaks for all studied compositions.

the volatilization loss. Firstly, $Mg(NO_3)_2 \cdot 6H_2O$ (≥99.0%), $Bi(NO_3)_3 \cdot 5H_2O$ (≥99.0%) and $Mn(NO_3)_2$ (49%∼51%) were dissolved in 2-methoxyethanol (2-MOE, ≥99.0%) in sequence. $Ti(OC_4H_9)_4$ (≥98.0%) was dissolved in 2-MOE using acetylacetone as the stabilizer and chelating agents. $Pb(OOCCH_3)_2 \cdot 3H_2O$ (≥99.0%) was dissolved in glacial acetic acid. Then, $Pb(OOCCH_3)_2$ solution was added to the $Ti(OC_4H_9)_4$ solution and stirred for 10 min. Subsequently, the above mixed solution was added into a mixed solution of $Mg(NO_3)_2$, $Bi(NO_3)_3$ and $Mn(NO_3)_2$ and simultaneously stirred to form a stable sol by adjusting the pH value of ∼5.4. Finally, an appropriate amount of N-N Dimethylformamide as a drying control chemical additive was added into the above solution to prevent the film from cracking. A little 2-MOE was added to adjust the viscosity and ultimately to form the BMT–0.37PT–*x*Mn precursor solution with a concentration of 0.2 M. After aging for 3∼5 days in air, the thin films were deposited onto Pt(1 1 1)/Ti/SiO_2/Si substrates by a repeated spin-coating process at 4000 rpm for 30 s. After each spin-coating step, the films were dried at 200 °C for 5 min, and pyrolyzed at 500 °C for 8 min under ambient atmosphere. Finally, the thin films were annealed at 675 °C for 30 min.

The phase structures were characterized by an X-ray diffractometer (XRD, D/MAX2500 V, Rigaku, Japan) with Cu Kα radiation. High-resolution X-ray photoelectron spectroscope (XPS, ESCALAB250, Thermo, America) was used to determine the valence states of Mn ions. The surface microstructure of BMT–0.37PT–*x*Mn thin films was observed by an atomic force microscope (AFM, Being Nano-Instruments CSPM-4000, Beijing, China). The dielectric properties (permittivity and loss tangent) as a function of frequency were measured by a precision impedance analyzer (HP 4194A, Hewlett-Packard, Palo Alto, CA). A ferroelectric testing system (Precision LC, Radiant Technologies Inc., Albuquerque, NM) was used to evaluate the ferroelectric properties and the leakage current characteristics of the thin films.

3. Results and discussion

3.1. XRD spectra

The XRD patterns of the BMT–0.37PT–*x*Mn thin films annealed at 675 °C for 30 min are shown in Fig. 1. The diffraction peaks were identified by using the standard powder diffraction data of pure PT. It is found that all the films consist of a single perovskite phase. The diffraction peak positions of the BMT–0.37PT–*x*Mn thin films are roughly in agreement with the standard diffraction peak positions of PT, indicating that the Mn doping does not change the perovskite structure of the film. However, as shown in Fig. 1 (b), the position of the (2 0 0) diffraction peak is shifted to a higher angle with increasing the Mn doping content up to 0.5 mol%, indicating that the unit cell volume is decreased. This can be attributed to the substitution of high-valance Mn ions (Mn^{3+} ∼0.58 Å, low spin for CN = 6; ∼0.645 Å, high spin for CN = 6; Mn^{4+} ∼0.53 Å, for CN = 6) for Ti^{4+} (∼0.605 Å, for CN = 6) [15]. However, as the Mn doping content increases from 0.5 mol% to 1 mol%, the position of the (2 0 0) peak does not change any more.

3.2. XPS spectra

In order to clarify the reason for the change of the peak position, the valence states of Mn ions for the 0.5 mol% and 1 mol% Mn doped BMT–0.37PT thin films were investigated by XPS. Fig. 2 shows Mn 2p XPS spectra of BMT–0.37PT–0.005 Mn and BMT–0.37PT–0.01Mn

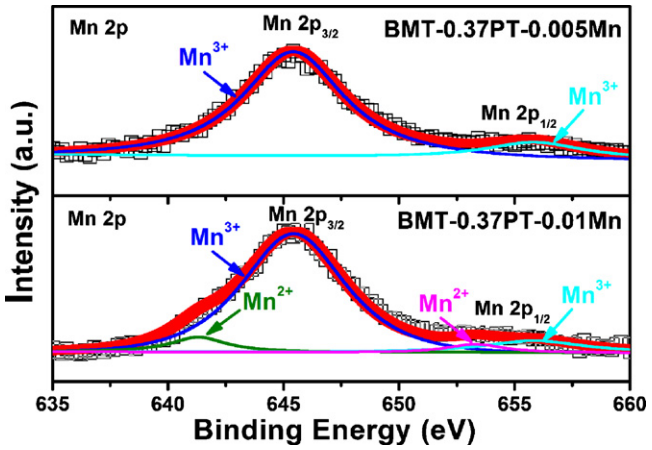

Fig. 2. X-ray photoelectron spectroscopic spectrum of Mn 2p for the BMT–0.37PT thin films doped with 0.5 mol% Mn and 1 mol% Mn. The "□" symbol represents the experimental data. The wide solid line represents the best fit to the experimental data. The thin solid lines represent the fitted multiple peaks.

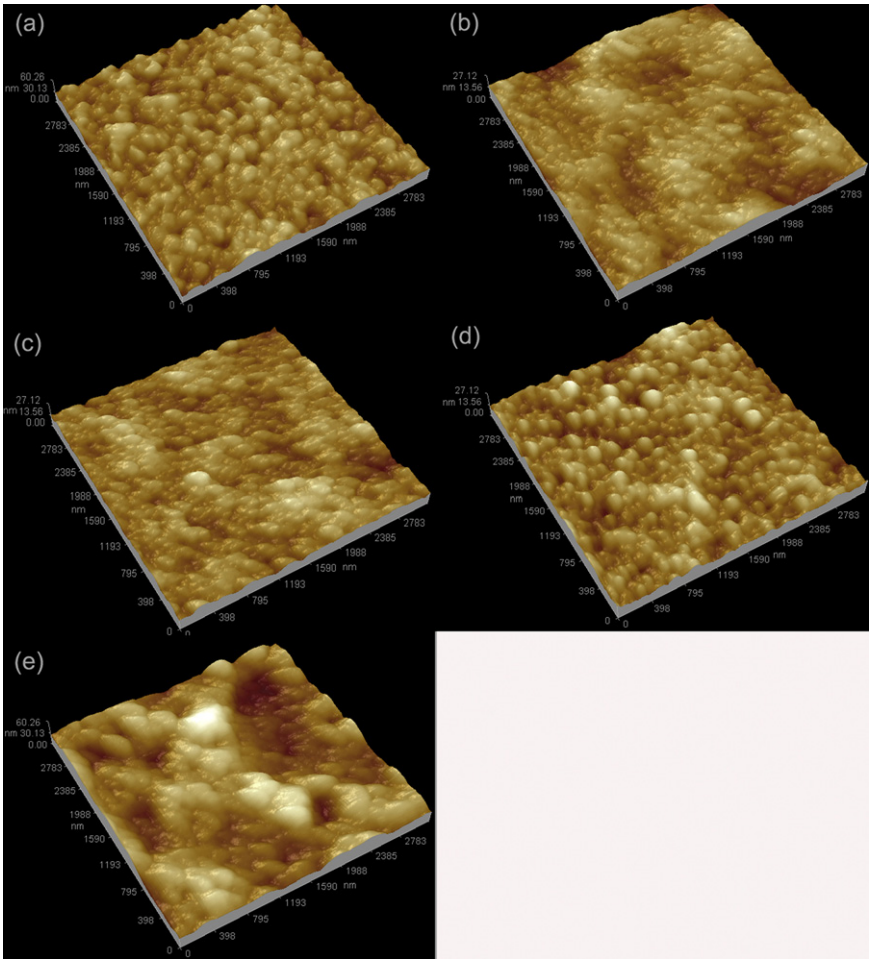

Fig. 3. Surface morphologies of BMT–0.37PT–*x*Mn thin films: (a) $x = 0.0$, (b) $x = 0.002$, (c) $x = 0.003$, (d) $x = 0.005$ and (e) $x = 0.01$.

samples. For the evaluation of the XPS data, the backgrounds have been subtracted from the spectra by the Shirley method [16], and the peaks were fitted by the software XPS-PEAK. It can be seen that for both spectra, the main peak located at about 645.3 eV should correspond to the $2p_{3/2}$ orbit peak of Mn^{3+}, and another peak at about 655.9 eV should be the $2p_{1/2}$ orbit peak of Mn^{3+} [17]. Compared to the 0.5% Mn doped sample, the 1 mol% Mn doped sample still has two extra peaks which correspond to the $2p_{1/2}$ orbit peak of Mn^{2+} at about 641.5 eV and 653.3 eV, respectively. Therefore, the shift of the diffraction peak position to higher angles can be attributed to the substitution of Mn^{3+} for Ti^{4+} as the Mn doping content increases to 0.5 mol%. However, the diffraction peak positions do not change as the Mn doping content increases from 0.5 mol% to 1 mol%. This is because Mn^{2+} (larger ionic radius) and Mn^{3+} (smaller ionic radius) substitute for Ti^{4+} simultaneously. However, the ionic radius of Mn^{2+} (0.67 Å, low spin for CN = 6; 0.83 Å, high spin for CN = 6) is larger than that of Ti^{4+} [15]. As a result, the substitution of Mn^{2+} for Ti^{4+} would be limited, so that some Mn^{2+} ions would remain at the grain boundary.

3.3. Morphology

Fig. 3 displays the surface morphology of the samples with different Mn-doping concentrations. It can be observed that the films with low Mn-doping contents exhibit a dense microstructure and a uniform grain size distribution. However, as the amount of Mn was further increased up to 1 mol%, inhomogeneous grain growth was observed. This may be due to the abnormal grain growth induced by the remaining Mn^{2+} ions at the grain boundary. Compared with the undoped BMT–0.37PT film, the grain size is smaller and the surface is more dense and smooth for films doped with a small amount of Mn. However, with the increase of the Mn doping content, the grain size increases. The possible reasons are given as follows: on the one hand, doping tends to change the crystallization process [18]. As Mn ions were doped in BMT–0.37PT, the crystallization mechanism could change from a homogeneous nucleation to a heterogeneous nucleation. The heterogeneous nucleation would promote the grain nucleation rate and simultaneously inhibit the grain growth, so that the grain size becomes smaller for the Mn doped samples; on the other hand, because Mn ions mainly exist in the state of Mn^{3+}, Mn^{3+} ions are likely to enter the B site to replace Ti^{4+}. To satisfy the requirement of charge neutrality, the extrinsic oxygen vacancies would be formed according to the following equation:

$$2Mn^{3+} + 2Ti^{4+} \rightarrow 2Mn'_{Ti} + 7O_O + V^{\bullet\bullet}_{OE} \quad (1)$$

where Mn'_{Ti} stands for a Mn^{3+} ion at a Ti^{4+} site, O_O strands for the oxygen ion on its normal site and $V^{\bullet\bullet}_{OE}$ stands for the extrinsic oxygen vacancy. The increased oxygen vacancies tend to promote the lattice diffusion, and thereby speed up the grain growth [19]. As shown in Fig. 1 (b), the diffraction peak position was shifted to the higher angle as Mn-doping contents increase to 0.5 mol%, indicating that more Mn^{3+} ions enter the B site. As a result, the grain size increases with the increase of the Mn doping content.

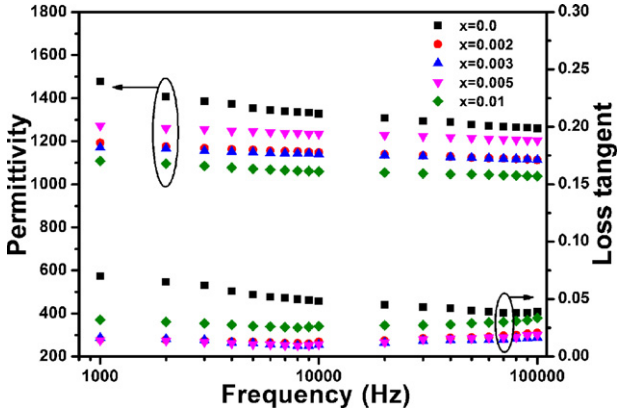

Fig. 4. The dielectric permittivity and loss tangent as a function of frequency for BMT–0.37PT–*x*Mn thin films as indicated.

3.4. Dielectric, ferroelectric and leakage current measurements

The frequency dependence of the dielectric permittivity and dissipation factor for the BMT–0.37PT–*x*Mn thin films is shown in Fig. 4. There is no sudden change of dielectric permittivity in the frequency range up to 100 kHz for Mn-doped BMT–0.37PT films. The dielectric permittivity exhibits a slight decline as the signal frequency increases from 1 kHz to 100 kHz. For the undoped BMT–0.37PT thin film, the dielectric permittivity declines distinctly at lower frequencies. This can be attributed to the reduced space charge polarization. The dielectric permittivity of Mn-doped BMT–0.37PT films is smaller than that of the undoped sample. This is a typical feature of the "hard" doping. The BMT–0.37PT–0.005Mn thin film demonstrates the largest dielectric permittivity among all Mn-doped samples. This might be due to the relatively large grain size for the 0.5 mol% Mn doped BMT–0.37PT film, as compared with other doped films in this study. However, for the BMT–0.37PT–0.01Mn film, the bad topography would result in the degradation of dielectric properties. The effect of the grain size on the electrical properties of thin films has been studied in our previous work [7]. In the low frequency range, the dissipation factors of Mn-doped BMT–0.37PT thin films are obviously reduced compared to those of the undoped film, although the surface topography of BMT–0.37PT–0.01Mn film is not dense enough. Mn doping effectively reduces the dielectric loss, meaning that the leakage current can be reduced by Mn doping.

Polarization versus electric filed (P–E) hysteresis loops of BMT–0.37PT–*x*Mn thin films are shown in Fig. 5. It can be found that saturated hysteresis loops are obtained for the Mn doped samples at a frequency of 100 Hz, while much higher frequencies are required for the undoped BMT–0.37PT thin film. The BMT–0.37PT–0.005Mn thin film measured at 100 Hz showed a more saturated hysteresis loop than the undoped one at 1 kHz, as can be seen from Fig. 5 (a). This means that the leakage current was reduced effectively by Mn doping. Fig. 5(b) shows the P–E loops measured at 100 Hz for BMT–0.37PT films doped with different contents of Mn. Compared with the undoped BMT–0.37PT thin film, the Mn doped samples show a decreased remanent polarization P_r and a reduced coercive field E_c. This is because the large leakage current for the undoped BMT–0.37PT film might result in a nonphysical increase of the remanent polarization and the coercive field [20]. With increasing the Mn doping content, the remanent polarization of the film decreases and the coercive field increases except for the BMT–0.37PT–0.005Mn film. Since Mn ions belong to acceptor dopants in this case, the formed oxygen vacancies would induce "hard" characteristics. In hard piezoelectric materials, ferroelectric domains are pinned by the internal bias field owing to defect dipoles caused by a non-centric distribution of oxygen vacancies

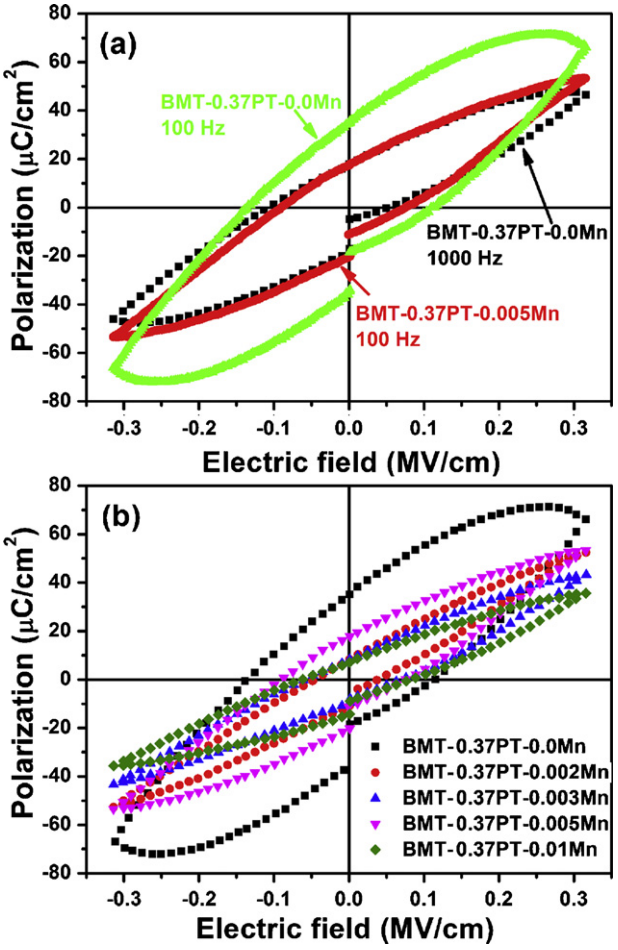

Fig. 5. P–E hysteresis loops of BMT–0.37PT–*x*Mn thin films (a) $x = 0.0$ and 0.005 at different signal frequencies, and (b) $x = 0.0$–0.01 at 100 Hz.

and dopants Mn ions [21,22]. As the Mn doping content increases, more ferroelectric domains are pinned. As a result, the switching of domains becomes harder. Therefore, the remanent polarization tends to decrease and the coercive field tends to increase. Similar to the result of dielectric properties, the BMT–0.37PT–0.005Mn thin film shows the optimum ferroelectric properties with the largest $P_r \sim 17.4\ \mu C/cm^2$ at 100 Hz, which is almost the same as that in the undoped film at 1 kHz. The P_r value of BMT–0.37PT–0.005Mn thin film is almost as same as that of the bulk ceramics ($P_r = 18\ \mu C/cm^2$) prepared by a solid-state reaction process with the addition of polyethylene glycol [22], and higher than that of bulk ceramics ($P_r = 7.9\ \mu C/cm^2$) fabricated by a conventional solid-state reaction method [8]. However, it is much lower than that of bulk ceramics ($P_r = 38\ \mu C/cm^2$) prepared by a high-pressure technique [6].

Fig. 6 shows the electric field dependence of the leakage current density of the undoped BMT–0.37PT and BMT–0.37PT–0.005Mn thin films. It is noticeable that the BMT–037PT–0.005Mn film shows lower leakage current density than the undoped sample. The leakage current density of both films increases gradually with increasing the applied electric fields. The current density of BMT–0.37PT–0.005Mn film is 3.1×10^{-5} A/cm^2 under an electric field of 0.2 MV/cm. Owing to the lead and bismuth volatilization during post annealing, intrinsic oxygen vacancies and free electrons are possibly formed according to the following equation:

$$O_O \leftrightarrow V_{OI}^{\bullet\bullet} + 2e' + 1/2O_2 \quad (2)$$

where $V_{OI}^{\bullet\bullet}$ denotes the intrinsic oxygen vacancy and e′ denotes the free electron. As demonstrated above, when Mn^{3+} acceptor replaces

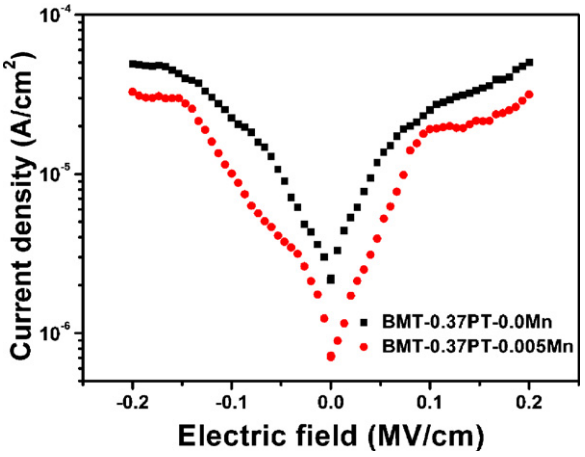

Fig. 6. Leakage current characteristics of undoped BMT–0.37PT and BMT–0.37PT –0.005Mn thin films.

Ti^{4+}, the extrinsic oxygen vacancy would be formed. As the substitution of Mn ions increases, the content of the extrinsic oxygen vacancy would increase. The increased oxygen vacancy eventually reduces the amount of both intrinsic oxygen vacancies and free electrons [14,23]. Therefore, the current density of the 0.5 mol% Mn doped BMT–0.37PT film can be significantly decreased as compared with that of the undoped thin film.

4. Conclusions

The BMT–0.37PT–*x*Mn thin films were fabricated by a sol–gel method on Pt(1 1 1)/Ti/SiO_2/Si substrates. The X-ray diffraction results indicate that the B-site Mn substitution does not change the perovskite structure of the films. The grain size was reduced by doping a small amount of Mn, whereas increased as the Mn doping content becomes more. Mn doping effectively enhances the resistivity and decreases the loss tangle of the films. The BMT–0.37PT–0.005Mn film shows lower leakage current density than the undoped BMT–0.37PT film such that saturated hysteresis loops can be obtained. The BMT–0.37PT–0.005Mn thin film exhibits the largest dielectric permittivity and remanent polarization in the doping concentration range.

Acknowledgements

This work was financially supported by a project of Natural Science Foundation of Anhui Province (1108085J14) and the National Natural Science Foundation of China (50972035 and 51272060).

References

[1] T. Yoshimura, S.T. Mckinstry, Growth and properties of (0 0 1) $BiScO_3$–$PbTiO_3$ epitaxial films, Applied Physics Letters 81 (2002) 2065–2066.
[2] H. Wen, X.H. Wang, C.F. Zhong, L.K. Shu, L.T. Li, Epitaxial growth of sol–gel derived $BiScO_3$–$PbTiO_3$ thin film on Nb-doped $SrTiO_3$ single crystal substrate, Applied Physics Letters 90 (2007), 202902-1-202902-3.
[3] M.A. Khan, T.P. Comyn, A.J. Bell, Large remanent polarization in ferroelectric $BiFeO_3$–$PbTiO_3$ thin films on Pt/Si substrates, Applied Physics Letters 91 (2007), 032901-1-032901-3.
[4] R.E. Eitel, C.A. Randall, T.R. Shrout, S.E. Park, Preparation and characterization of high temperature perovskite ferroelectrics in the solid solution $(1-x)$ $BiScO_3$–$xPbTiO_3$, Japanese Journal of Applied Physics 41 (2002) 2099–2104.
[5] S.M. Choi, C.J. Stringer, T.R. Shrout, C.A. Randall, Structure and property investigation of a Bi-based perovskite solid solution: $(1-x)$ $Bi(Ni_{1/2}Ti_{1/2})O_3$ –$xPbTiO_3$, Journal of Applied Physics 98 (2005), 034108.
[6] C.A. Randall, R. Eitel, B. Jones, T.R. Shrout, Investigation of a high T_c piezoelectric system: $(1-x)Bi(Mg_{1/2}Ti_{1/2})O_3$–$xPbTiO_3$, Journal of Applied Physics 95 (2004) 3633–3639.
[7] L.D. Liu, R.Z. Zuo, Fabrication and electrical properties of sol–gel-derived $0.63Bi(Mg_{1/2}Ti_{1/2})O_3$–$0.37PbTiO_3$ thin films, Journal of the American Ceramic Society 94 (2011) 3686–3689.
[8] R. Rai, A. Sinha, S. Sharmac, N.K.P. Sinham, Investigation of structural and electrical properties of $(1-x)Bi(Mg_{0.5}Ti_{0.5})O_3$–$xPbTiO_3$ ceramic system, Journal of Alloys and Compounds 486 (2009) 273–277.
[9] T. Mihara, H. Watanable, Electronic conduction characteristics of sol–gel ferroelectric $Pb(Zr_{0.4}Ti_{0.6})O_3$ thin-films capacitors: part II, Japanese Journal of Applied Physics 34 (1995) 5674–5682.
[10] J.L. Chen, H.M. Chen, J.Y.M. Lee, An investigation on the leakage current and time dependent dielectric breakdown of ferroelectric lead–zirconate–titanate thin films capacitors for memory device applications, Applied Physics Letters 69 (1996) 4011–4013.
[11] A. Morelli, S. Venkatesan, G. Palasantzas, B.J. Kooi, J.T.M. De Hosson, Polarization retention loss in $PbTiO_3$ ferroelectric films due to leakage currents, Journal of Applied Physics 102 (2007), 084103.
[12] M. Abazari, E.K. Akdogan, A. Safaria, Effect of manganese doping on remnant polarization and leakage current in $(K_{0.44},Na_{0.52},Li_{0.04})(Nb_{0.84},Ta_{0.10},Sb_{0.06})O_3$ epitaxial thin films on $SrTiO_3$, Applied Physics Letters 92 (2008), 212903.
[13] W. Sakamoto, A. Iwata, T. Yogo, Ferroelectric properties of chemically synthesized perovskite $BiFeO_3$-$PbTiO_3$ thin films, Journal of Applied Physics 104 (2008), 104106.
[14] Y.Y. Wu, X.H. Wang, C.F. Zhong, L.T. Li, Effect of Mn doping on microstructure and electrical properties of the $(Na_{0.85}K_{0.15})_{0.5}Bi_{0.5}TiO_3$ thin films prepared by sol–gel method, Journal of the American Ceramic Society 94 (2011) 3877–3882.
[15] R.D. Shannon, Revised effective ionic radii and systematic studies of interatomic distances in halides and chalcogenides, Acta Crystallographica Section A. Crystal Physics, Diffraction, Theoretical and General Crystallography 32 (1976) 751–767.
[16] D.A. Shirley, High-resolution X-ray photoemission spectrum of the valence bands of gold, Physical Review B 5 (1972) 4709–4714.
[17] B.S. Li, Z.G. Zhu, G.R. Li, A.L. Ding, Microstructure and electromechanical properties in PMnN-PZT ceramics sintered at different temperatures, Journal of Materials Sciences & Technology 21 (2005) 386–390.
[18] P.Y. Du, L.W. Tang, X.H. Zhao, W.J. Weng, G.R. Han, Effect of Tb^{3+} doping on the preferred orientation of lead titanate thin film prepared by sol–gel method on ITO/glass substrates, Surface and Coatings Technology 198 (2005) 395–399.
[19] H.Y. Park, C.H. Nam, I.T. Seo, J.H. Choi, S. Nahm, Effect of MnO_2 on the piezoelectric properties of the $0.75Pb(Zr_{0.47}Ti_{0.53})O_3$–$0.25Pb(Zn_{1/3}Nb_{2/3})O_3$ ceramics, Journal of the American Ceramic Society 93 (2010) 2537–2540.
[20] R. Meyer, R. Waser, Dynamic leakage current compensation in ferroelectric thin-film capacitor structures, Applied Physics Letters 86 (2005), 142907.
[21] S. Takahashi, Effects of impurity doping in lead zirconate–titanate ceramics, Ferroelectrics 41 (1982) 143–156.
[22] S.H. Yu, Y. Ye, H.T. Huang, L.M. Zhou, Z.Q. Wang, Preparation, structure and properties of $Bi(Mg_{1/2}Ti_{1/2})$–$PbTiO_3$ ceramics and Mn-doping effect, Proceedings of SPIE 6423 (2007), 64234H.
[23] S.S. Kim, Leakage current behaviors of acceptor and donor doped $Ba_{0.5}Sr_{0.5}TiO_3$ thin films, Applied Physics Letters 75 (1999) 2554–2556.